JOURNAL OF CATALYSIS **178,** 441–449 (1998)
ARTICLE NO. CA982149

Interaction of Oxygen with Pure and SrO-Doped Nd_2O_3 Catalysts for the Oxidative Coupling of Methane: Study of Work Function Changes

G. Gayko,[1] D. Wolf,[2] E. V. Kondratenko,[3] and M. Baerns[2,4]

Lehrstuhl für Technische Chemie, Ruhr-Universität Bochum, D-44780 Bochum, Germany

Received August 5, 1997; revised March 3, 1998; accepted May 4, 1998

For the oxidative coupling of methane a relationship between the state of surface oxygen and C_2 selectivity of Nd_2O_3 and SrO (1 at%)/Nd_2O_3 catalysts was derived from contact potential differences (CPD) between a reference electrode and the catalyst surface as a function of oxygen partial pressure and temperature. The influence of the concentration of oxygen anion vacancies of the oxide lattice on the state of surface oxygen was elucidated by measurements of the electrical conductivity and of isotopic oxygen exchange on the undoped and SrO-doped Nd_2O_3. Oxygen defects facilitate the oxygen incorporation into the lattice of SrO(1 at%)/Nd_2O_3 as indicated by the lower CPD changes due to oxygen adsorption and the higher extent of oxygen exchange for SrO-doped Nd_2O_3 compared with pure Nd_2O_3. Thus, the C_{2+} selectivity of a SrO(1 at%)/Nd_2O_3 catalyst was enhanced since the concentration of weakly adsorbed (molecular) oxygen species leading to deep oxidation of hydrocarbons is lower on a defect rich solid surface. © 1998 Academic Press

Key Words: **oxidative coupling of methane; surface oxygen on Nd_2O_3-based catalysts; work function as mean of catalyst-surface characterization; isotopic oxygen exchange; electrical conductivity of Sr-doped neodymia.**

INTRODUCTION

In the selective oxidation of hydrocarbons the interaction of the catalyst with adsorbed oxygen comprises an electron transfer from the catalytic solid to the adsorbate; charged surface-oxygen species can activate C-C or C-H bonds of the hydrocarbon. The nature of such chemisorbed oxygen entities depends on oxygen partial pressure, temperature and physical properties of the catalytic material (1). Oxygen chemisorption is assumed to be mainly influenced by the availability of electrons (semiconductivity) in the catalyst and its ability to build up a dynamic equilibrium between gas phase, surface, and bulk lattice oxygen (the latter being determined by oxygen anion conductivity). Doping of a solid material often changes its electronic properties and its catalytic performance concomitantly.

In the oxidative coupling of methane (OCM) to ethane rare-earth oxides doped with small amounts of alkaline-earth oxides have been found among the best catalysts with respect to selectivity and activity (2, 3). Substitution of rare-earth cations by alkaline-earth cations leads to structural defects in the oxygen sublattice. Anshits as well as Baerns and their co-workers have recently emphasized the availability of oxygen defects as a major catalyst feature for the OCM reaction in two review articles (4, 5). By analysis of electrical conductivity data Baerns *et al.* indirectly concluded that a high concentration of oxygen vacancies promotes the transformation of adsorbed oxygen species into lattice oxygen (5–8). Correspondingly, adsorption of molecular oxygen as electrophilic entities (O_2^-, O_2^{2-}) is expected to be small on anion vacancy-rich surfaces (4). However, direct evidence for this conclusion was not available yet. Moreover, the nature of the oxygen species activating methane is still a question of controversy (2, 5).

The work-function increase resulting from the formation of negative charges due to oxygen adsorption on a metal oxide surface as measured by a Kelvin probe renders it possible to observe the adsorption process (9). The method is based on the determination of the contact potential difference (CPD) between a reference electrode (e.g., gold) and the catalyst surface, the materials together forming a dynamic condenser.

In the present work this method was applied to further elucidate the relationship between the state and type of surface oxygen and the C_2 selectivity of pure and SrO-doped Nd_2O_3 in the OCM reaction.

To support the interpretation of work function changes caused by variation of the oxygen partial pressure at different temperatures alternating current (ac) conductivity data as well as the degree of isotopic exchange between gasphase $^{18}O_2$ and surface ^{16}O were determined. These methods allow conclusions concerning the defect structure and the oxygen mobility inside the oxide catalysts.

[1] Present address: Ichthyol Company, Scientific Department, Sportallee 85, D-22335 Hamburg, Germany.

[2] Present address: Institute for Applied Chemistry Berlin-Adlershof e. V., Rudower Chaussee 5, D-12484 Berlin, Germany.

[3] On leave: Russian Academy of Sciences, Institute of Chemicals of Natural Organic Materials, Krasnojarsk.

[4] To whom correspondence should be addressed.

0021-9517/98 $25.00

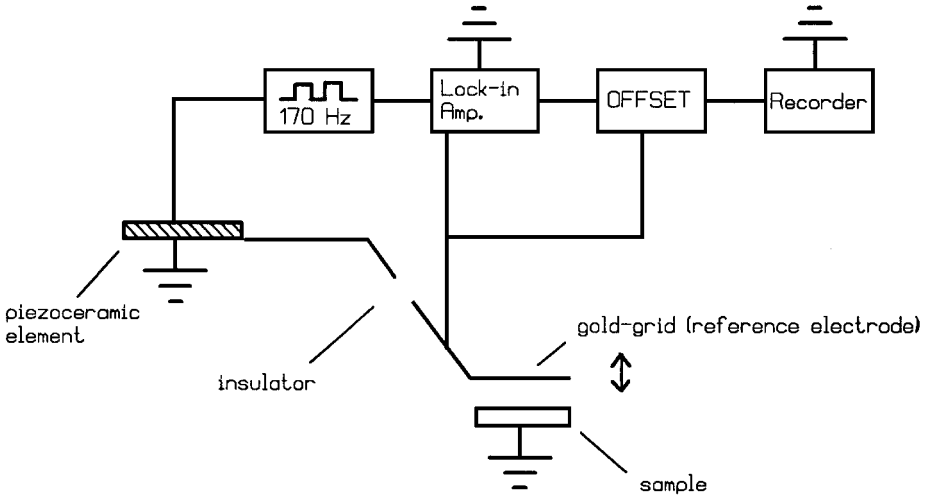

FIG. 1. Experimental setup for CPD measurements.

METHOD

In the following section the background for interpretation of results of CPD and electrical conductivity measurements is summarized. Especially, the relationship between the process of oxygen adsorption and/or incorporation, change of work function, defect structure of oxides as well as type of electrical conductivity and its corresponding experimental identification are referred to.

CPD Measurements

The experimental setup is shown schematically in Fig. 1. Contact-potential differences between the oxide catalyst and a reference electrode (gold-grid) are measured by means of a Kelvin probe (Besocke/Delta-Phi-Elektronik, probe "S" (10)) with a 2.5-mm diameter gold-grid vibrating condenser element.

The CPD values are obtained from the compensation of the difference in work function between the catalyst and the reference electrode. Additional charges on the surface of the catalyst caused by adsorption of gas molecules alter its work function and, hence, the CPD. If the adsorption capacity of the reference electrode is negligible, the work function changes of the investigated sample (ϕ_s) are equal to the changes of the CPD:

$$\Delta\mathrm{CPD} \cong \Delta\phi_s. \qquad [1]$$

Gold as reference material is known to be inert against oxygen at room temperature; at higher temperatures it interacts with oxygen as a function of oxygen partial pressure (11, 12). However, for pressures below 5×10^{-3} Pa pure gold surfaces may serve as inert reference electrodes at temperatures up to 800 K (13, 14). For this reason, CPD measurements were carried out in a vacuum chamber.

Since the piezoceramic driven Kelvin probe used in this study is not applicable at temperatures higher than 520 K for CPD measurements up to 800 K, the sample was solely heated through its metallic support by means of a tungsten filament (see Fig. 2). Temperatures were measured on the surface of the metallic support by means of a spot-welded thermocouple.

Information on the charge of surface oxygen species may be derived according to Barbaux *et al.* (15, 16) and Nowotny

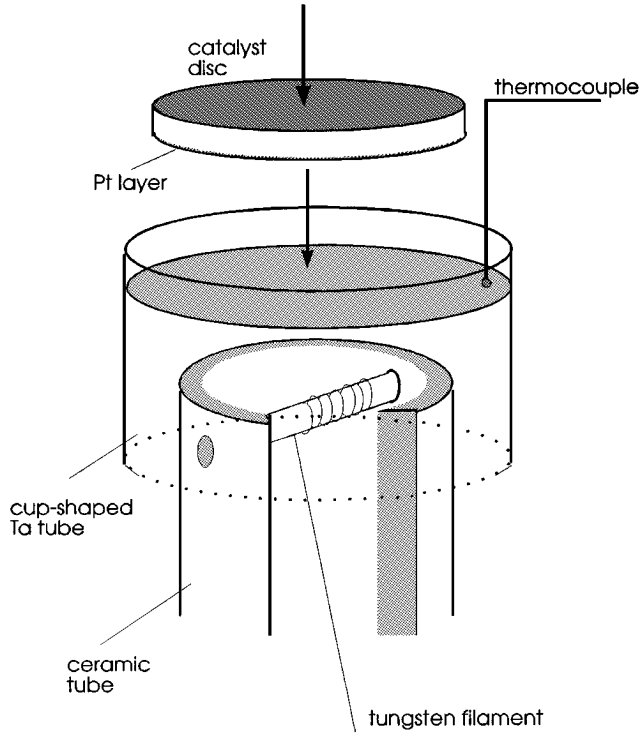

FIG. 2. Scheme of the sample holder for CPD measurements.

(17) in a metal-oxide/oxygen system from Eq. [2]:

$$CPD = \frac{k \cdot T}{a \cdot e} \ln p_{O_2} + \text{const.} \qquad [2]$$

In this equation a gives the number of electrons transfered from the solid to the adsorbed oxygen species. I.e., changes in CPD caused by variations in oxygen partial pressure at constant temperature are directly related to the charge of surface oxygen entities like O_2^-, O^-, and O^{2-}, resulting from the adsorption equilibrium expressed by Eq. [3] with $h^\bullet$ being the positive holes according to Kröger Vink notation (18) and $a = 2n/m$:

$$O_{2,g} \rightleftarrows \frac{2}{m} O^{n-}_{m,\,ads} + \frac{2n}{m} h^\bullet \qquad [3]$$

Conductivity Measurements

A metal oxide catalyst may simultaneously show several types of conductivities (n- and p-type, respectively, plus oxygen–anion conductivity). In some (straightforward) cases the value of each kind of conductivity can be derived by evaluating ac electrical conductivity data obtained at different oxygen partial pressures. p-type conductivity is present if the conductivity σ increases with increasing partial pressure of oxygen ($\delta\sigma/\delta p_{O2} > 0$). It is usually found at much higher p_{O2} than n-type conductivity which is indicated by a decrease of conductivity with increasing oxygen partial pressure ($\delta\sigma/\delta p_{O2} < 0$). In an intermediate pressure range oxygen anions may be the dominant charge carriers ($\delta\sigma/\delta p_{O2} = 0$) (5).

The proportion of ionic conductivity σ_{ion} can be determined from evaluation of the total conductivity (σ_{tot}) as function of oxygen partial pressure. Since the ionic conductivity is independent of oxygen partial pressure, the intersection of the functional relationship between σ_{tot} and $p_{O2}^{1/n}$ with the ordinate is equal to σ_{ion}. According to Eq. [4] (19, 20) the theoretical value of n is 4, if the activation of oxygen proceeds via anion vacancies resulting in O^{2-} species:

$$\sigma_{tot} = \sigma_{ion} + k p_{O2}^{1/4}. \qquad [4]$$

Thus, from the experimental value of n the mechanism of oxygen incorporation into the oxide lattice can be derived.

EXPERIMENTAL

Catalyst Preparation and Characterization

$SrO(1\ at\%)/Nd_2O_3$ ($S_{BET} = 1.3\ m^2g^{-1}$) was prepared by coprecipitation of a continuously stirred nitrate solution of neodymium and strontium with 1 M oxalic acid at room temperature. After 2 h of stirring subsequent to coprecipitation the slurry was allowed to settle overnight. The precipitate was then filtered and washed with oxalic acid. Then it was dried at 120°C for 4 h and calcined at 1123 K for 24 h in ambient air. The atomic surface concentration of Sr (Sr/(Sr + Nd)) amounted to 3.3% for doped Nd_2O_3 as determined by XPS. There was no other phase detected than the type A of rare earth oxides by XRD. Pure Nd_2O_3 ($S_{BET} = 0.8\ m^2g^{-1}$) was obtained by precipitation from the nitrate solution and subsequent treatment as described above. Catalyst pellets pressed from the ground powders at 2.2×10^5 Pa for 20 s were crushed and sieved to a grain fraction of 0.355 to 0.500 mm for catalyst testing.

Catalyst Testing

A catalytic fixed bed reactor (8 mm ID) made of quartz was used. For temperature control the reactor was immersed into a fluidized bed of sand. The product gas, from which water was removed by condensation, was analyzed by g.c. (for specific conditions see (7, 8)). The OCM reaction was performed at 923–1023 K; the feed gas consisted of methane (60 kPa), oxygen (6 kPa), and nitrogen (34 kPa). The modified contact time ($m_{cat}/\dot{V}_{STP}$) was varied by charging different amounts of catalyst at a constant flow rate of 3.2 ml/s.

CPD Measurements

The powdered catalyst samples were pressed into flat specimens of 0.42–0.45 mm thickness and Ø 7 mm. One side of the pellet was covered with a platinum paste (Heraeus) that was burned together with the oxide sample at 973 K for 30 min to ensure the intimate electrical contact of the sample with the support it was placed on. In the experimental studies the interaction of oxygen with the catalyst sample was studied at temperatures between ca 400 and 780 K applying oxygen partial pressures between 1×10^{-4} and 5×10^{-3} Pa. Partial pressures of oxygen were adjusted by a dosing valve, starting at a base pressure of approximately 2×10^{-5} Pa.

Pretreatment of samples was carried out at 673 K and an oxygen partial pressure of 1.0×10^{-2} Pa. After cooling to the measuring temperature the oxygen partial pressure was decreased to 2×10^{-4} Pa. After establishing a constant CPD signal, work function changes were caused by successively increasing the oxygen partial pressure. At each level of oxygen partial pressure the CPD change was recorded up to the steady state. The corresponding CPD values were used for data evaluation according to Eq. [2].

Oxygen Exchange

Oxygen-exchange measurements between gas-phase $^{18}O_2$ and the metal-oxide surfaces of Nd_2O_3 and SrO $(1\ at\%)/Nd_2O_3$ at temperatures ranging from 523 to 873 K were performed under vacuum conditions in the Temporal Analysis of Products (TAP) reactor as explained by Buyevskaya *et al.* (21). An amount of 0.6 g of the respective oxides was packed between two layers of quartz of the same particle size. To remove water from the catalyst

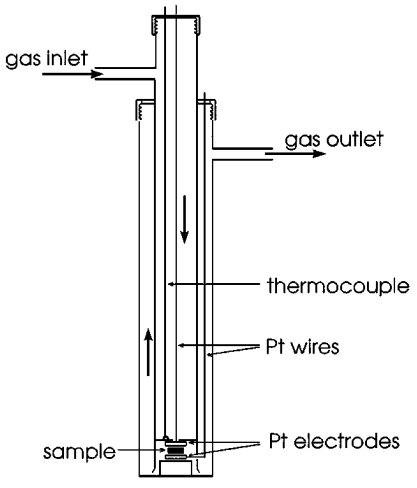

FIG. 3. Scheme of the quartz cell used for measurements of conductivity.

it was first exposed to the base pressure of the system (ca 10^{-4} Pa) at 1023 K. Then the temperature was lowered to the respective temperatures at which $^{16}O_2$ was pulsed until a stable response was observed at the reactor outlet. Thus, an oxygen-saturated surface was preserved as initial state of the oxygen exchange experiments. $^{18}O/^{16}O$ exchange rate was determined by pulsing an $^{18}O_2 : Ne = 1:1$ mixture over the catalysts, one pulse containing approximately 10^{15} molecules of $^{18}O_2$.

Conductivity Measurements

The total conductivity (*n*- and *p*-type, respectively, plus oxygen anion conductivity) of catalysts consisting of Nd_2O_3 and SrO (1 at%)/Nd_2O_3 were determined by measuring the specific resistance of a catalyst disc with the two-electrode ac method (5). For this purpose ac (1 kHz) measurements were performed with an automatically compensating bridge (Wayne Kerr B905) with two inert platinum electrodes arranged in a quartz cell (see Fig. 3). As an equivalent circuit a parallel connection of a condenser and an ohmic resistance was applied (22).

The ground powders were pressed to pellets of 7-mm diameter at a pressure of 2.2×10^5 kPa. To minimize contact resistances the discs were covered by a platinum paste on each side and were burned for 30 min at a temperature of 1023 K. Ac conductivity measurements were carried out as a function of temperature ($T = 673$–1023 K) and of oxygen partial pressure ($p_{O2} = 0.1$–31.6 kPa).

RESULTS AND DISCUSSION

First, the results of catalytic measurements are presented. CPD measurements of pure and doped Nd_2O_3 are discussed with reference to the catalytic results in order to derive conclusions concerning the influence of oxygen adsorption and incorporation on the catalyst performance. To support these conclusions results of conductivity and oxygen exchange measurements were taken into account providing additional information on the extent of oxygen incorporation and defect structure of the oxides.

Catalyst Performance

The promoting effect of doping Nd_2O_3 with SrO on selectivity to ethane, ethylene, and minor amounts of C_3 hydrocarbons ($S_{C_{2+}}$) at otherwise comparable reaction conditions is illustrated in Table 1. Over the whole temperature range C_{2+} selectivity is the highest for Nd_2O_3 doped with SrO.

The plot of C_2-selectivity versus oxygen conversion (Fig. 4) illustrates the relation between the rates of primary C_2 product formation and the consecutive oxidation of ethane and ethylene which corresponds to the sudden drop of selectivity at high oxygen conversion. For the undoped sample this drop already occurs at 85% oxygen conversion, whereas the C_2 selectivity of the SrO(1 at%)/Nd_2O_3 catalysts increases up to 90% conversion of oxygen (see also (23)). I.e., the consecutive oxidation of C_2 hydrocarbons is suppressed to a certain extent when Nd_2O_3 has been doped with SrO.

Indications that the extent of consecutive oxidation is strongly related to the state of surface oxygen on basic

TABLE 1

Catalytic Performance of Nd_2O_3 and SrO (1 at%)/Nd_2O_3 in the Oxidative Coupling of Methane ($p^0_{CH4} = 60$ kPa, $p^0_{O2} = 6$ kPa, $p_{N2} = 34$ kPa)

	T /K	τ /g · s · ml^{-1}	O_2 conversion /%	CH_4 conversion /%	C_{2+} selectivity /%
Nd_2O_3	923	0.0738	88.9	7.3	18.0
	973	0.0700	97.5	9.3	35.0
	1023	0.0333	97.0	10.9	50.6
SrO (1 at%)/Nd_2O_3	923	0.0554	89.5	8.2	34.3
	973	0.0525	97.0	10.7	51.8
	1023	0.0333	97.4	12.5	63.8

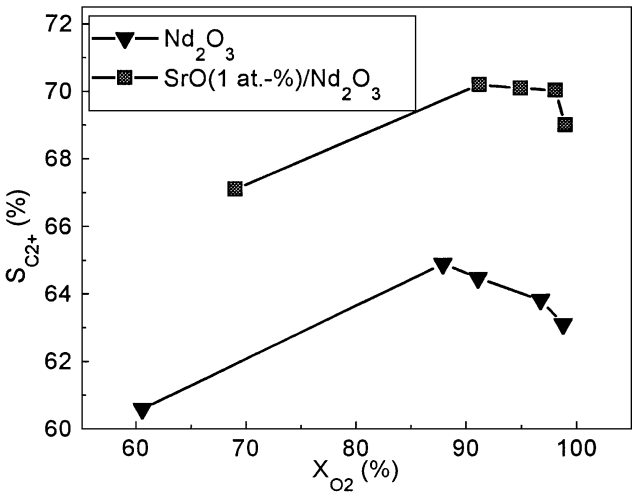

FIG. 4. Dependence of C_{2+} selectivity on oxygen conversion. Reaction conditions: temperature 1023 K, $CH_4/O_2/N_2 = 60/6/34$, modified contact time 0.004. 0.008, 0.016, 0.02, and 0.028 $g \cdot s \cdot ml^{-1}$.

oxides result from earlier work of Lunsford *et al.* (24). The authors reported that the reaction of O_2^- on a MgO surface is significantly faster with C_2 and C_3 hydrocarbons than with CH_4. Furthermore, the chain length of carboxylates which are surface intermediates in the reaction of alkanes and alkenes with O^-, O_2^-, and O_3^- were degraded after interaction with O_2^- and O_3^- but not after interaction with O^-. Therefore, the oxygen species consisting of more than one oxygen atom should especially promote C-C bond disruption being probably the initial step of C_2 combustion. The concentration of multi-atomic oxygen species should be diminished if a high concentration of oxygen vacancies on the surface is available which accelerates the dissociation of oxygen. Whether these relationships do indeed play a role for the Nd_2O_3 and the (SrO 1 at%)/Nd_2O_3 catalyst should be investigated by the CPD measurements presented in the following paragraph.

Work Function Changes

A successive enhancement of oxygen partial pressure starting from 2×10^{-4} Pa leads to a steplike increase of the work function as illustrated for Nd_2O_3 at 523 K in Fig. 5a. The CPD change decreases with increasing temperature (Fig. 6). At similar temperatures the CPD change is much smaller for SrO (1 at%)/Nd_2O_3 than for undoped Nd_2O_3. A facilitated mobility of defects can be made responsible for the steep drop of CPD change with growing temperature for the SrO-doped sample.

As mentioned in the section "Method" information on the charge of surface oxygen species might be derived according to Barbaux *et al.* (15, 16) and Nowotny (17) in a metal–oxide/oxygen system from Eq. [2]. Application of Eq. [2] to the data in Fig. 5a obtained at 523 K leads to the straight lines shown in Fig. 5b. From the slope of this plot coefficients *a* of equal to 0.31 and 0.22 result. Obviously, these values do not correspond to a particular partially reduced oxygen species since for O_2^-, O^-, or O^{2-} values of *a* between 1 and 4 would be expected.

However, with increasing temperature CPD changes become smaller and the coefficient *a* increases as illustrated for Nd_2O_3 at 673 K in Fig. 7.

The values of *a* could be interpreted in such a way that previously adsorbed molcular oxygen which is nearly uncharged is transformed to O_3^-, O_2^-, O^-, and O^{2-} at higher temperatures. Such a development of coefficient *a* with increasing temperature was also observed by Cherrak *et al.* on pure Sm_2O_3 (25). At higher oxygen partial pressures they found by CPD measurements that only lattice oxygen

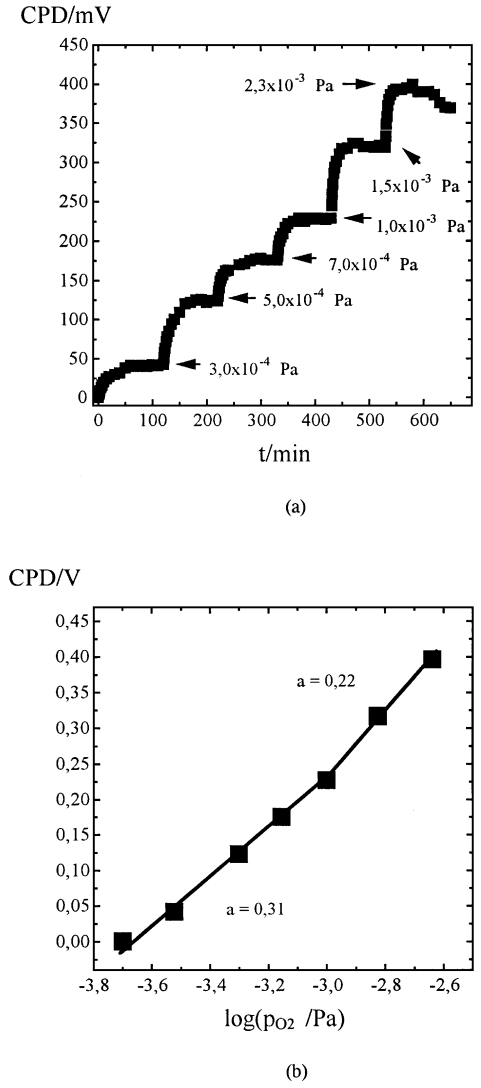

FIG. 5. (a) Contact potential difference as a function of time for undoped Nd_2O_3 at 523 K after stepwise change of oxygen partial pressure; (b) CPD change (height of the different steps in (5a) as function of $\log(p_{O_2}/Pa)$ for Nd_2O_3 at 523 K.

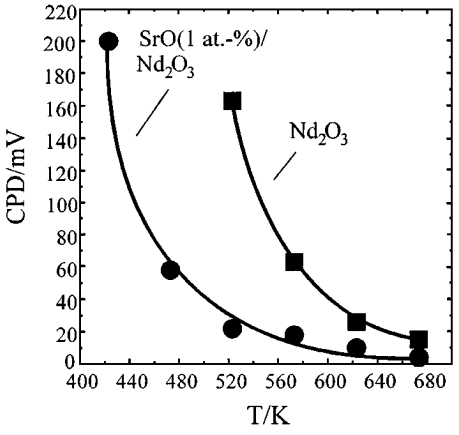

FIG. 6. Comparison of work function changes as a function of temperature upon oxygen exposure to Nd_2O_3 and SrO (1 at%)/Nd_2O_3 ($1.0 \times 10^{-3} \rightarrow 2.0 \times 10^{-3}$ Pa).

is present on the surface of Sm_2O_3 at temperatures higher than approximately 650 K.

For SrO (1 at%)/Nd_2O_3 the development of coefficient a with increasing temperature is similar to that on undoped Nd_2O_3. However, at the same temperature it is always larger for the SrO-doped sample than for the pure neodymia as summarized in Table 2.

This result indicates that oxygen dissociates on the surface of SrO (1 at%)/Nd_2O_3 at lower temperatures than on undoped Nd_2O_3. Oxygen is already transformed to lattice oxygen at temperatures between 623 K and 673 K.

Especially at low oxygen partial pressure ($2.0 \times 10^{-4} < p_{O2} < 1.0 \times 10^{-3}$ Pa) and high temperature (400°C), where the concentration of oxygen vacancies is expected to be high, values higher than 4 occur which are not meaningful from the physicochemical point of view. However, under these conditions the CPD changes are very small and the signal-to-noise ratio is high, leading to large experimental errors as illustrated by the confidence intervals in Table 2.

To further elucidate these findings pulse experiments on ^{18}O exchange were performed, giving information on the rate of interaction of the gas phase oxygen with lattice oxygen.

TABLE 2

Coefficient a for Nd_2O_3 and SrO (1 at%)/Nd_2O_3 in Dependence on Temperature

T/K	a(Nd_2O_3)	a(SrO(1 At.-%)/Nd_2O_3)
423	—	$0{,}21 \pm 0{,}02$
473	—	$1{,}10 \pm 0{,}36$
523	$0{,}31 \pm 0{,}01^a$; $0{,}22 \pm 0{,}01^b$	$4{,}97 \pm 0{,}10^a$; $1{,}52 \pm 0{,}05^b$
573	$0{,}62 \pm 0{,}04^c$	$1{,}91 \pm 0{,}12$
623	$1{,}26 \pm 0{,}09^b$	$3{,}08 \pm 0{,}08$
673	$2{,}73 \pm 0{,}29^c$	$6{,}0 \pm 2{,}4$

[a] $2{,}0 \times 10^{-4} < p_{O2} < 1{,}0 \times 10^{-3}$ Pa.
[b] $p_{O2} \geq 1{,}0 \times 10^{-3}$ Pa.
[c] $p_{O2} \geq 5{,}0 \times 10^{-4}$ Pa.

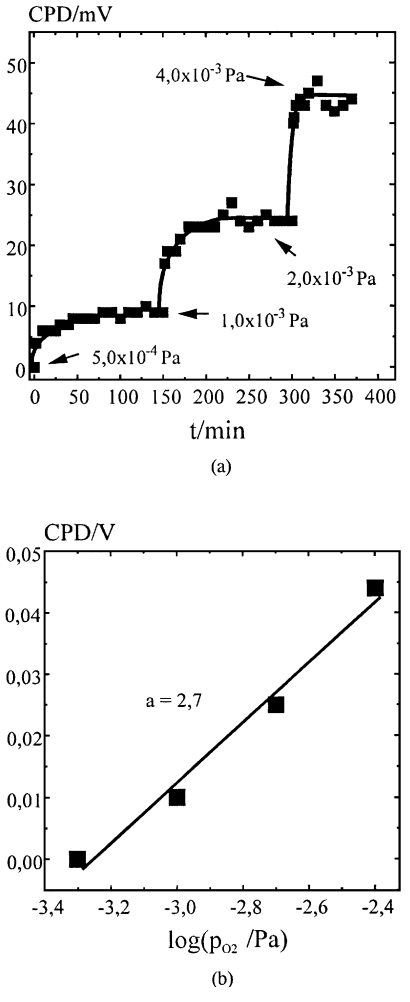

FIG. 7. (a) Contact Potential Difference as a function of time for undoped Nd_2O_3 at 673 K after stepwise change of oxygen partial pressure. (b) Plot of CPD (height of the different steps in (7a) as a function of log(pO_2/Pa) for Nd_2O_3 at 673 K.

Oxygen Exchange

For the SrO-doped sample rate of oxygen isotopic exchange as expressed by the $^{18}O_2$ conversion during the first pulse starts above 523 K and reaches more than 90% at 773 K (see Fig. 8). At isothermic reaction conditions the $^{18}O_{2,g}$ conversion is 15 to 30% higher for the doped sample than for the undoped one between 623 and 773 K. For pure Nd_2O_3 at 823 K it still has not reached 90%.

Comparable results were obtained by Kalenik and Wolf, who doped La_2O_3 with 1 at% SrO (26), and by Peil *et al.*, who added Li to MgO (27). Zhang *et al.*, as well as Anshits and co-workers, pointed out that the increase of the diffusion coefficient of lattice oxygen (O^{2-}) correlates with the enhanced oxygen exchange properties of the doped

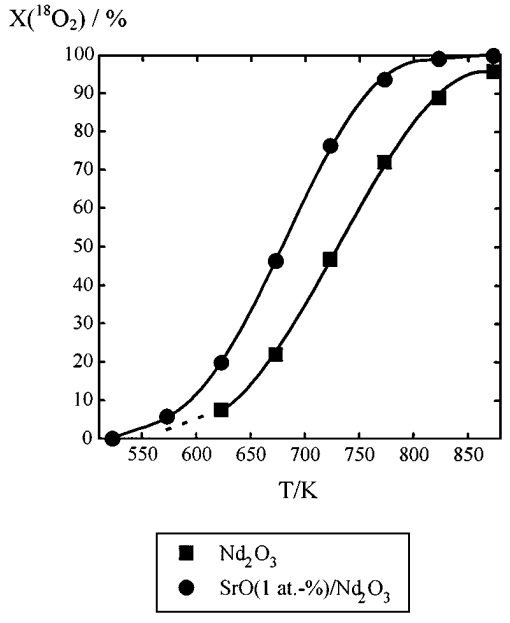

FIG. 8. Conversion of $^{18}O_2$ in $^{18}O/^{16}O$ exchange for Nd_2O_3 and SrO (1 at%)/Nd_2O_3 as a function of temperature.

oxides (4, 5). Since the diffusion coefficient, in turn, is a function of oxygen defect concentration, the above-mentioned results confirm the higher concentration of oxygen-anion vacancies in SrO (1 at%)/Nd_2O_3, compared with Nd_2O_3. Therefore, oxygen vacancies should promote oxygen dissociation and concomitantly increase the C_2 selectivity. More detailed information on the defect structure of the oxides can be derived by the measurements of electrical conductivity.

Electrical Conductivity

Doping Nd_2O_3 with SrO resulted in an increase of overall conductivity by approximately two orders of magnitude as indicated by ac measurements (see Figs. 9a and b). The increase of conductivity with growing oxygen partial pressure indicates the presence of positive holes as dominating charge carriers in both samples resulting in *p*-type conductivity.

For *p*-type conductors the process of oxygen incorporation can be described by Eq. [5], where gas-phase oxygen occupies oxygen vacancies. Positive holes are formed in this process, the conductivity increases with increasing oxygen partial pressure (according to Kröger–Vink notation (18): $V_O^{\cdot\cdot}$ = oxygen vacancies, $h^\bullet$ = positive holes, $O_O^\bullet = O^-$ species at a lattice site, O_O^x = atomic lattice oxygen).

$$0.5O_{2,g} + V_O^{\cdot\cdot} \leftrightarrow O_O^x + 2h^\bullet. \qquad [5]$$

Additional oxygen vacancies would be generated by doping Nd_2O_3 with strontium if Sr^{2+} occupies regular Nd^{3+} cationic positions as proposed by Sinev *et al.* (28) (Eq. [6a]). In this case, the deficiency of a positive charge in the cationic sublattice is counter balanced by the formation of positive holes (either $h^\bullet$ or $O_O^\bullet$) and atomic lattice oxygen (O_O^x), due to simultaneous oxygen incorporation (Eq. [6b]):

$$2SrO \leftrightarrow 2Sr'_{Nd} + V_O^{\cdot\cdot} + 2O_O^x \qquad [6a]$$

$$0.5O_{2,g} + V_O^{\cdot\cdot} \leftrightarrow O_O^x + 2h^\bullet. \qquad [6b]$$

Oxygen incorporation according to Eqs. [5] and [6b] would result in an exponent of $n = 4$ and the total conductivity would be described by Eq. [4].

The experimental values do confirm this mechanism of incorporation for both Nd_2O_3 as well as SrO (1 at%)/Nd_2O_3 since the plot σ versus $\log(p_{O2})^{1/4}$ shows a clear linear dependency (Fig. 10). Moreover, the higher value of the intersection with the σ-axis for the doped sample indicates the

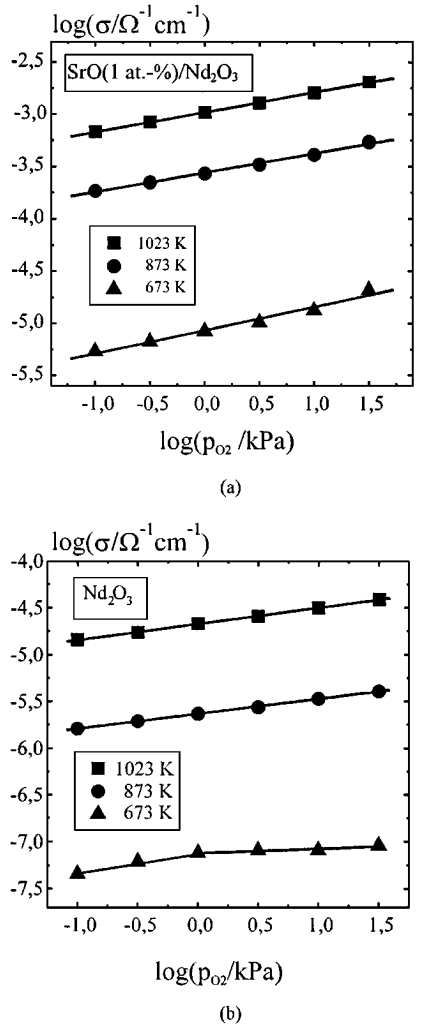

FIG. 9. Conductivity of (a) SrO(1 at%)/Nd_2O_3 and (b) Nd_2O_3 at 673, 873, and 1023 K as a function of oxygen partial pressure.

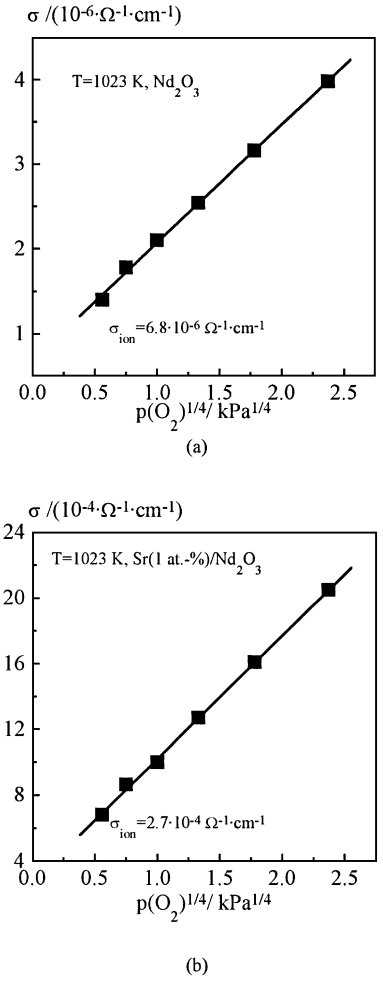

FIG. 10. Total conductivity depending on $p_{O2}^{1/4}$ at 1023 K, (a) Nd_2O_3, (b) SrO (1 at%)/Nd_2O_3.

higher oxygen anion conductivity, i.e. higher concentration of oxygen vacancies than pure Nd_2O_3.

Thus, the measurements of conductivity also support the CPD results concerning the accelerated incorporation of oxygen and electron transfer to the oxygen species due to doping.

CONCLUSIONS

The investigation of catalytic performance, measurements of CPD, oxygen exchange activity, as well as electrical conductivity, leads to a consistent picture on the role of different oxygen species in the oxidative coupling of methane.

Doping Nd_2O_3 with SrO leads to a suppression of catalyst activity in secondary combustion of C_2 hydrocarbons which is caused by a change of the state of surface oxygen.

Conductivity data and oxygen exchange properties of SrO (1 at%)/Nd_2O_3 point towards the generation of oxygen defects by doping. Oxygen-anion vacancies make possible the oxygen dissociation and movement of oxygen through the solid at much lower temperatures than for pure Nd_2O_3. For this reason the incorporation of adsorbed oxygen species is facilitated for the SrO-doped sample. This was directly seen by CPD measurements as a function of temperature. There is a strong indication by CPD studies that the extent of oxygen incorporation into the lattice is increased with increasing temperature. The layer of adsorbed oxygen species and the corresponding charge accumulation in the boundary layer between bulk and surface ("Randschicht") for SrO (1 at%)/Nd_2O_3 is reduced at lower temperatures, compared with Nd_2O_3. Although work function studies were carried out under reduced pressure, this leads to the assumption that under OCM reaction conditions weakly bound surface oxygen entities are transformed into lattice oxygen much faster for a defect solid like SrO-doped Nd_2O_3 than for pure neodymia. Against this background the C_{2+} selectivity of SrO (1 at%)/Nd_2O_3 is enhanced because the concentration of multi-atomic surface oxygen species leading to deep oxidation of hydrocarbons is smaller. However, this does not necessarily mean that lattice oxygen is responsible for methane activation. According to conductivity data positive holes are the dominating charge carriers in SrO (1 at%)/Nd_2O_3. Positive holes may be identical with positively charged (O^-) lattice oxygen in equilibrium with lattice oxygen (O^{2-}). Against these results the opposing views of homolytic versus heterolytic splitting of a C-H bond in methane activation for forming CH_3 species may be reconciled by assuming that O^- and strongly nucleophilic O^{2-} species contribute to both types of splitting process.

ACKNOWLEDGMENT

The financial support of this work by Deutsche Forschungsgemeinschaft (Contract Ba262/10-1) and the discussion with Dr. Diana Filkova of the Institute of Catalysis of the Bulgarian Academy of Science have been greatly appreciated. E. V. Kondratenko thanks the Alexander-von-Humboldt-Stiftung for supporting his scientific work in Germany.

REFERENCES

1. Bielanski, A., and Haber, J., "Oxygen in Catalysis," Marcel Dekker, New York, 1991.
2. Lunsford, J. H., *Stud. Surf. Sci. Catal.* **81**, 1 (1994).
3a. Mleczko, L., and Baerns, M., *Fuel Process. Technol.* **42**, 217 (1995).
3b. Becker, S., and Baerns, M., *J. Catal.* 512 (1993).
4. Voskresenskaya, E. N., Roguleva, V. G., and Anshits, A. G., *Catal. Rev.-Sci. Eng.* **37**(1), 101 (1995).
5. Zhang, Z., Verykios, X. E., and Baerns, M., *Catal. Rev.-Sci. Eng.* **36**(3), 507 (1994).
6. Zhang, Z., and Baerns, M., *J. Catal.* **135**, 317 (1992).
7. Borchert, H., Gayko, G., and Baerns, M., *Chem.-Ing.-Tech.* **66**, 343 (1994).
8. Borchert, H., and Baerns, M., *J. Catal.* **168**, 315 (1998).
9. Nowotny, J., and Sloma, M., *Mater. Sci. Monogr.* **47**, 281 (1998).
10. Besocke, K., and Berger, S., *Rev. Sci. Instrum.* **47**, 840 (1976).

11. Sachtler, W. M. H., Dorgelo, G. J. H., and Holscher, A. A., *Surf. Sci.* **5**, 221 (1996).
12. Sazonova, I. S., and Keier, N. P., *Kinet. and Catal.* **6**, 390 (1965).
13. Eley, D. D., and Moore, P. B., *Surf. Sci.* **76**, L599 (1978).
14. Pireaux, J. J., Chtaib, M., Delrue, J. P., Thiry, P. A., Liehr, M., and Caudano, R., *Surf. Sci.* **141**, 211 (1984).
15. Barbaux, Y., Bonnelle, J.-P., and Beaufils, J.-P., *J. Chem. Res.* **M**, 556 (1979).
16. Grzybowska, B., Barbaux, Y., and Bonnelle, J. P., *J. Chem. Res.* **M**, 650 (1981).
17. Nowotny, J., *Mat. Sci. Monogr.* **15**, 358 (1982).
18. Kröger and Vink, *Solid State Phys.* **3**, 307 (1956).
19. Jahnke, H., Moro, B., Dietz, H., and Beyer, B., *Ber. Bunsenges. Phys. Chem.* **92**, 1250 (1988).
20. Subbarao, E. C., and Maiti, H. S., *Solid State Ionics* **11**, 317 (1984).
21. Buyevskaya, O. V., Rothaemel, M., Zanthoff, H. W., and Baerns, M., *J. Catal.* **150**, 71 (1994).
22. Kudo, T., and Fueki, K., "Solid State Ionics," Verlag Chemie, Weinheim, 1990.
23. Filkova, D., Wolf, D., Gayko, G., Baerns, M., and Petrov, L., *Appl. Catal. A* **159**, 33 (1997).
24. Iwamoto, M., and Lunsford, J.-H., *J. Phys. Chem.* **84**, 3079 (1980).
25. Cherrak, A., Hubaut, R., and Barbaux, Y., *J. Chem. Soc. Faraday Trans.* **88**(21), 3241 (1992).
26. Kalenik, Z., and Wolf, E. E., *Catal. Lett.* **11**, 309 (1991).
27. Peil, K. P., Goodwin, J. G., and Marcelin, G., *J. Phys. Chem.* **93**, 5977 (1989).
28. Sinev, M. Yu., Tulenin, Yu. T., Kalashnikova, O. V., and Shiryaev, P. A., in "Presentation, 5th European Workshop Meeting on Selective Oxidation by Heterogeneous Catalysis, Berlin, Nov. 6 & 7, 1995," p. 61.